

Combustion synthesis and characterization of Sm³⁺ and Tm³⁺ co-activated yttrium orthovanadate phosphate

Selepe Joel Motloun^{1*}, Kamohelo George Tshabalala¹, Odireleng Martin Ntwaeaborwa^{2*}

¹Department of Physics, University of the Free State (Qwa-Qwa Campus), Private Bag X 13, Phuthaditjhaba, 9866, South Africa

²School of Physics, University of the Witwatersrand, Private Bag 3, Wits, 2050, South Africa

*Corresponding author, E-mail: ntwaeab@gmail.com; tlousj@gmail.com

Received: 17 September 2016, Revised: 04 November 2016 and Accepted: 20 November 2016

DOI: 10.5185/amlett.2017.1405

www.vbripress.com/aml

Abstract

Samarium (Sm³⁺) and thulium (Tm³⁺) co-activated yttrium orthovanadatephosphate YV_{0.5}P_{0.5}O₄: Sm³⁺, Tm³⁺ powder phosphors were synthesized by solution combustion method and were annealed at 900°C for 2 hours. The x-ray diffraction patterns confirmed that the tetragonal structure of YV_{0.5}P_{0.5}O₄ was crystallized. The patterns consisted of peaks from YVO₄ and YPO₄ suggesting that our product was an admixture of both compounds. The scanning and transmission electron microscopy image showed an agglomeration of particles with different sizes and shapes. The UV-vis reflectance spectra showed a broad absorption band extending from 200 — 550 nm associated with the O→V charge transfer transitions of [VO₄]³⁻. The photoluminescence (PL) data of singly doped phosphors showed one blue emission peak at 477 nm (¹G₄—³H₆) and three emission peaks at 567 nm (⁶G_{5/2}—⁶H_{5/2}), 603 nm (⁶G_{5/2}—⁶H_{7/2}) and 650 nm (⁶G_{5/2}—⁶H_{9/2}) corresponding to transitions of Tm³⁺ and Sm³⁺ ions respectively. The PL data from the Sm³⁺- Tm³⁺ co-doped systems demonstrated an enhancement of visible emission of Tm³⁺ by down-conversion process that involves energy capture by the host last and Sm³⁺ that was subsequently transferred to Tm³⁺. These materials are evaluated as possible candidates to improve the power conversion efficiency of dye sensitized solar cells. Copyright © 2017 VBRI Press.

Keywords: Orthovanadatephosphate, phosphors, photoluminescence, down-conversion, energy transfer.

Introduction

Yttrium orthophosphate (YPO₄) and orthovanadates (YVO₄) have been investigated for a long time because of their interesting properties such as excellent thermal and chemical stability among other things [1-3]. They are also excellent host lattices for rare earth ions to produce a variety of light emitting materials with high luminescence quantum yields and emission originating from the f-f transitions [4-7] and high absorption coefficients at pumping wavelengths. YVO₄ belongs to tetragonal crystal, and has similar structure as ZrSiO₄. In this structure, 4 oxygen atoms occupy every vanadium atom, 8 oxygen atoms occupy every yttrium atom and 8 oxygen atoms form 2 distorted tetrahedron [8]. YPO₄ also belongs to tetragonal system with zircon type structure, with 4 oxygen atoms occupying every phosphorus atom, 8 oxygen atoms occupying every yttrium atom, and 8 oxygen atoms forming two distorted tetrahedron [9].

Research has shown that the stability and high temperature luminescent properties of YVO₄ or YPO₄ can be improved by partial replacement of the [VO₄]³⁻ with [PO₄]³⁻ ions (or [PO₄]³⁻ with [VO₄]³⁻) to form a multicomponent system called yttrium orthovanadatephosphate (YV, PO₄) [10]. Depending on

the annealing temperature, this system can also crystallize in a tetragonal structure and it is an excellent host for rare earth ions. Various methods have been used before to synthesize multicomponent structures of yttrium orthovanadatephosphate [11 - 14]. In this work, solution combustion method was used to prepare samarium (Sm³⁺) and thulium (Tm³⁺) co-activated yttrium orthovanadatephosphate (YV_{0.5}P_{0.5}O₄: Sm³⁺, Tm³⁺) phosphor that can be used as down-converters in dye sensitized solar cells (DSSCs). With the growing requirements in global renewable energy, dye sensitized solar cells (DSSC) have been widely studied as alternatives for the generation of electricity from sunlight due to their relatively high performance and simple production process [14]. Recently, Zhao and his group [16], have reported the conversion efficiency in DSSCs of up to 48%. These solar cells can only absorb in the visible region and other wavelengths like energy rich ultraviolet radiation are wasted. Furthermore, the degradation of the solar cell due to the incidence of UV radiation is an important detrimental factor that reduces its efficiency [17]. These drawbacks can be fixed by the coating with a down-conversion or up-conversion phosphor material layer that has the potential to enhance the efficiency of DSSCs by converting ultraviolet or near infrared radiation

to visible emission [18]. That is, coating DSSC with these phosphor materials will increase their absorption range and make them harvest more light and therefore improve their power conversion efficiency [19]. However, we will not report on the application of $YV_{0.5}P_{0.5}O_4: Sm^{3+}, Tm^{3+}$ in DSSCs.

Experimental

The starting materials: AR grade 99.99% yttrium nitrate hexahydrate ($Y(NO_3)_3 \cdot 6H_2O$), ammonium metavanadate (NH_4VO_3), ammonium phosphate ($NH_4H_2PO_4$), urea (CH_4N_2O), samarium nitrate hexahydrate ($Sm(NO_3)_3 \cdot 6H_2O$) and thulium nitrate hexahydrate ($Tm(NO_3)_3 \cdot 6H_2O$) were purchased from sigma Aldrich and were used without further purification.

Samarium and/or thulium activated yttrium vanadate-phosphate $YV_{0.5}P_{0.5}O_4: x \text{ mol } \% Sm^{3+}$ ($x = 1, 2 \text{ and } 3$) phosphors were synthesized by solution combustion method using urea as a fuel. In a typical procedure, stoichiometric amounts of yttrium nitrate ($Y(NO_3)_3 \cdot 6H_2O$), ammonium metavanadate (NH_4VO_3), ammonium phosphate ($NH_4H_2PO_4$), Samarium nitrate ($Sm(NO_3)_3 \cdot 6H_2O$) and urea (CH_4N_2O) were dissolved in 15 ml of deionized water in different glass beakers. The mixtures were stirred on a magnetic hotplate at a temperature of $\pm 70^\circ C$ until homogeneous solutions are obtained. The solutions were then transferred into different crucibles and subsequently transferred into a muffle furnace preheated to a temperature of $600 \pm 10^\circ C$.

As a result of exothermic reaction that took place, the final products were fluffy ashes. The resulting combustion ashes were then cooled down in air at room temperature and were manually ground gently using pestle and mortar to obtain a fine powder. The synthesized powders were then annealed in air at $900^\circ C$ for 2 hours. The same procedure was used for the synthesis of thulium activated yttrium vanadate-phosphate $YV_{0.5}P_{0.5}O_4: x \text{ mol } \% Tm^{3+}$ ($x = 1, 2 \text{ and } 3$) and samarium/thulium doubly doped yttrium vanadate-phosphate $YV_{0.5}P_{0.5}O_4: x \text{ mol } \% Sm^{3+}, y \text{ mol } \% Tm^{3+}$.

The XRD spectra were recorded using Siemens D5000 powder Diffractometer. The X-ray radiation used during the measurement was a $CuK\alpha$ source ($\lambda = 1.5406 \text{ \AA}$). Reflectance spectra were measured using UV-vis spectrophotometer Lambda 950 (PerkinElmer). The photoluminescence (both excitation and emission) data were recorded using a Hitachi F700 fluorescence spectrophotometer. The morphology and elemental composition of the materials were obtained using Jeol JSM-7800F field emission scanning electron microscope (FE-SEM) fitted with Oxford Aztec 350 X-Max80 energy-dispersive X-ray spectroscopy (EDS) and a high-resolution transmission electron microscope (HR-TEM) JEOL JEM 2100.

Results and discussion

Fig. 1(a) shows the XRD patterns of $YV_{0.5}P_{0.5}O_4: Sm^{3+}, Tm^{3+}$ powder phosphors annealed at $900^\circ C$ for 2 hours. The XRD spectra show diffraction peaks associated with YVO_4 (JCPDS file no. 17 – 0341) and YPO_4 (JCPDS file

no. 11 – 0254) and this suggests that $YV_{0.5}P_{0.5}O_4$ is an admixture of YVO_4 and YPO_4 components.

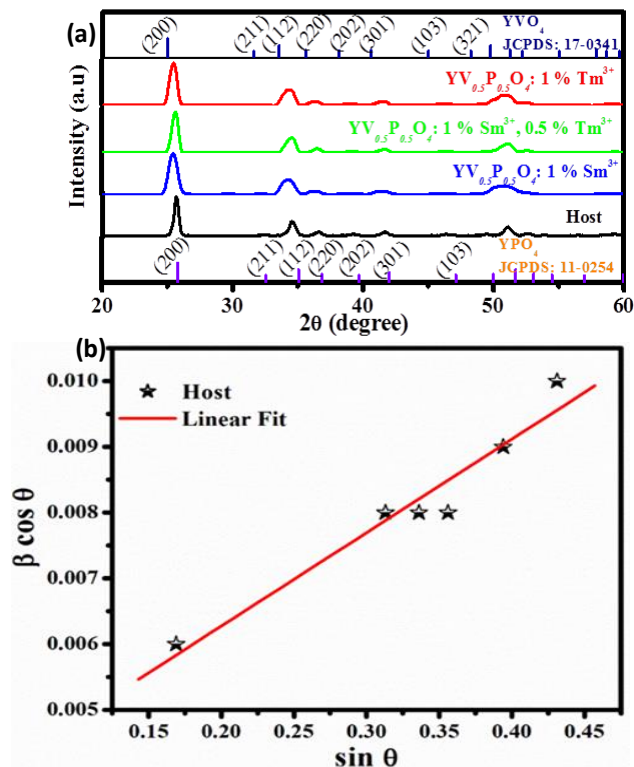


Fig. 1. (a). XRD patterns of $YV_{0.5}P_{0.5}O_4$ host, singly doped $YV_{0.5}P_{0.5}O_4: 1 \text{ mol } \% Sm^{3+}, 1 \text{ mol } \% Tm^{3+}$ and co-doped $1 \text{ mol } \% Sm^{3+}; 0.5 \text{ mol } \% Tm^{3+}$, (b). A plot of $\beta \cos \theta$ against $\sin \theta$ of $YV_{0.5}P_{0.5}O_4$ (host).

Table 1. Estimated lattice strain and the crystallite sizes of $YV_{0.5}P_{0.5}O_4$, $YV_{0.5}P_{0.5}O_4: 1 \text{ mol } \% Sm^{3+}$, $YV_{0.5}P_{0.5}O_4: 1 \text{ mol } \% Tm^{3+}$ and $YV_{0.5}P_{0.5}O_4: 1 \text{ mol } \% Sm^{3+}; 0.5 \text{ mol } \% Tm^{3+}$

Sample	D (nm)	η
$YV_{0.5}P_{0.5}O_4$	46.10	1.694×10^{-2}
$YV_{0.5}P_{0.5}O_4: 1 \text{ mol } \% Tm^{3+}$	63.36	2.739×10^{-2}
$YV_{0.5}P_{0.5}O_4: 1 \text{ mol } \% Sm^{3+}$	95.70	4.645×10^{-2}
$YV_{0.5}P_{0.5}O_4: 1 \text{ mol } \% Sm^{3+}; 0.5 \text{ mol } \% Tm^{3+}$	73.81	3.759×10^{-2}

Furthermore, the result indicates that the powder phosphors were crystalline and the diffraction peaks were broadened which is an indication that the average crystallite size was small. The lattice strain and the crystallite sizes were estimated from Williamson-Hall formula:

$$\beta \cos \theta = \eta \sin \theta + \frac{0.9\lambda}{D} \quad (1)$$

where, D is the crystallite size, η is the lattice strain, λ is the wavelength of the X-ray radiation (1.5418 \AA), β is the full width at half maximum and θ is the diffraction angle at the peak position. A plot of $\beta \cos \theta$ versus $\sin \theta$ of undoped $YV_{0.5}P_{0.5}O_4$ is presented in **Fig. 1(b)**. The lattice strain was estimated from the slope of the graph while the crystallite size was estimated from the y-intercepts. The estimated lattice strain and crystallite size of un-doped $YV_{0.5}P_{0.5}O_4$, and of either Sm^{3+}/Tm^{3+} single doped and $Sm^{3+}-Tm^{3+}$ co-doped $YV_{0.5}P_{0.5}O_4$ are presented

in **Table 1**. As evident from the table, the host has the least crystallite size with less lattice strain while the doped and doubly doped samples have larger size with higher lattice strain. The increase in lattice strain is assumed to be the result of difference in ionic radii of Y and the dopants (i.e. Tm and Sm).

Fig. 2 shows the SEM image of $YV_{0.5}P_{0.5}O_4$: 3 mol % Sm^{3+} , 2.5 mol % Tm^{3+} phosphor powder prepared by solution combustion method before annealing (a) and after annealing at 900 °C for 2 hours (b and c). The SEM image of the un-annealed phosphor powder shows that the powder is agglomerated with 3D structures of various shapes orderly build on top of each other forming thick sheets. On the other hand, annealed phosphor powder consists of non-agglomerated 3D structures of various shapes which includes among others, spheres, ovals and cuboids.

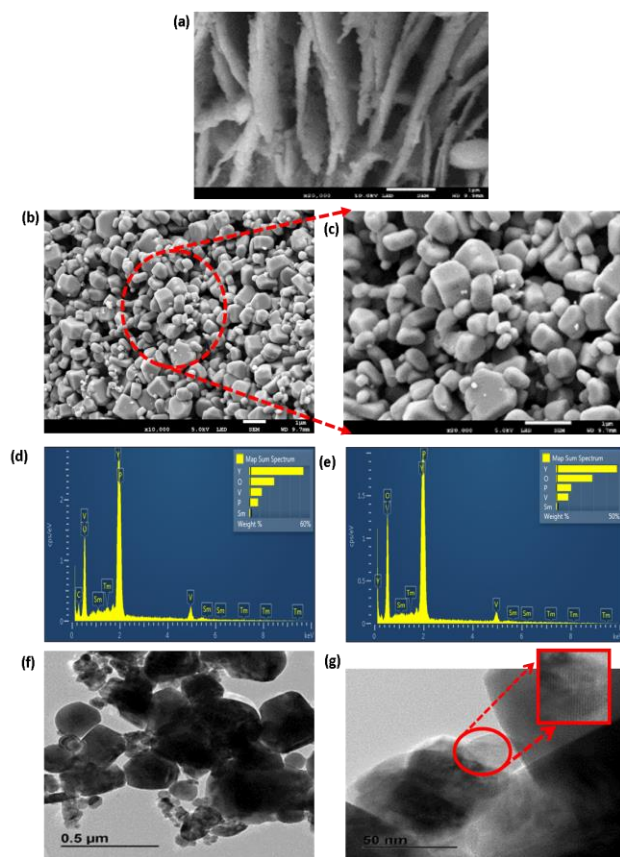


Fig. 2. (a) Unannealed (b) and (c) annealed: SEM micrographs of $YV_{0.5}P_{0.5}O_4$: 3 mol % Sm^{3+} , 2.5 mol % Tm^{3+} . Low (d) and high (e) magnification TEM images of $YV_{0.5}P_{0.5}O_4$: 3 mol % Sm^{3+} , 0.25 mol % Tm^{3+} . EDS spectra of $YV_{0.5}P_{0.5}O_4$: 3 mol % Sm^{3+} , 2.5 mol % Tm^{3+} (f) unannealed (g) annealed.

Furthermore, the particles have different sizes and are less agglomerated. To further investigate the surface morphology transmission electron microscopy (TEM) was used. **Fig. 2** (d) and (e) shows the energy dispersive X-ray spectroscopy (EDS) spectrum of $YV_{0.5}P_{0.5}O_4$: 3 mol % Sm^{3+} , 2.5 mol % Tm^{3+} . The spectra for both annealed and un-annealed show the presence of major elements, namely, Y, V, P, O, Sm and Tm. The atomic ratio of Y, V, P, O, Sm and Tm is approximately 49:28:11:09:2. In figure 2(f) there are some traces of carbon, which is not

associated with our sample in this case, but it is assumed to have come from the carbon tape used to mount the sample. **Fig. 2** (f and g) present the TEM images of $YV_{0.5}P_{0.5}O_4$: 3 mol % Sm^{3+} , 2.5 mol % Tm^{3+} phosphor powder. The particles are agglomerated and they have various sizes and shapes (**Fig. 2(f)**). Furthermore, it can also be observed that resolved lattice fringes were formed, confirming that the powder has high level of periodicity and therefore highly crystalline. This is evident from **Fig. 2** (g) and this is consistent with the obtained XRD results.

Fig. 3 presents the room temperature reflectance spectra of $YV_{0.5}P_{0.5}O_4$: x mol % Sm^{3+} ($x = 1, 2, 3$). The spectrum in **Fig. 3(a)** displays a plateau of high reflection in the wavelength range of 550–800 nm. The broad absorption band ranging from 200–550 nm with maximum absorption at ~ 300 nm was observed and it is attributed to the $O \rightarrow V$ charge transfer transitions of $[VO_4]^{3-}$ [20, 21]. According to the literature [21], V atoms occupy three different sites V1, V2 and V3, all of which consists of $[VO_4]$ tetrahedral. Therefore, this absorption band must come from the combination of $O - V1$, $O - V2$ and $O - V3$ charge transfer transitions [21, 22]. In **Fig. 3(a)**, (b) and (c) respectively, a similar trend was observed except for the additional small band at ~ 692 nm. This small band, which increases with the concentration of Tm^{3+} , corresponds to ${}^3H_6 - {}^3F_3$ transition of Tm^{3+} [23]. The estimated band gaps as shown in figure 3 (d) range between 2.5 to 3.3 and 3.2 to 3.4 nm for 3 mol % Sm^{3+} ; x mol % Tm^{3+} and 1 mol % Tm^{3+} ; x mol % Sm^{3+} respectively.

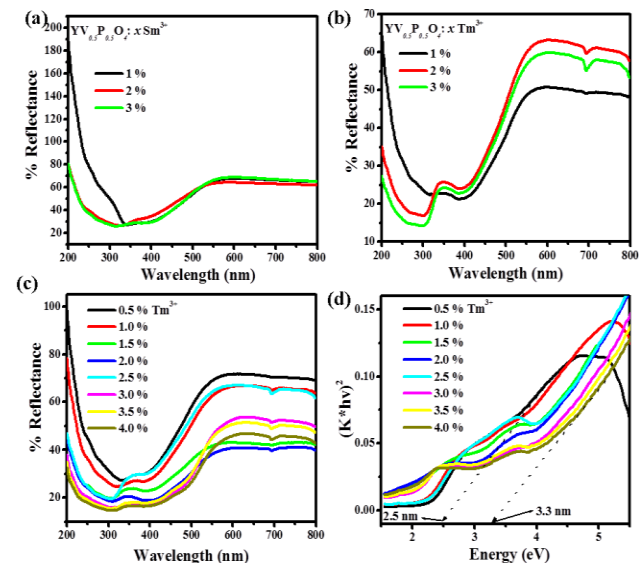


Fig. 3. UV-vis reflectance spectra of (a) $YV_{0.5}P_{0.5}O_4$: x mol % Sm^{3+} , (b) x mol % Tm^{3+} , (c) 3 mol % Sm^{3+} ; x mol % Tm^{3+} and (e) 1 mol % Tm^{3+} ; x mol % Sm^{3+} . (d) Transformed Kubelka-Munk reflectance spectrum of 3 mol % Sm^{3+} ; x mol % Tm^{3+} , and (f) 1 mol % Tm^{3+} ; x mol % Sm^{3+} .

Fig. 4(a) show the excitation spectra of $YV_{0.5}P_{0.5}O_4$: x mol % Tm^{3+} ($x = 0, 1, 2, 3$) phosphors obtained by monitoring the emission wavelength at 477 nm. The excitation spectra show two strong broad bands in the UV region. The band extending from 200 to 230 nm is attributed to host absorption [13] while the one between 230 and 350 nm with the maximum at 280 nm is ascribed

to $Tm^{3+} - O^{2-}$ charge transfer bands [11,24, 25]. Figure 4(b) show the emission spectra of $YV_{0.5}P_{0.5}O_4: x \text{ mol } \% Tm^{3+}$ ($x=0, 1, 2, 3$). The emission spectra were recorded when the phosphor powders were excited with a wavelength of 280 nm. The spectra exhibit similar trend with a broad band ranging from 400 to 550 nm and one dominant blue peak at around 477 nm for Tm^{3+} doped samples. These bands are ascribed to host emission peak and $^1G_4 - ^3H_6$ transition of Tm^{3+} respectively. Figure 4(c) shows the intensity of blue emission ($^1G_4 - ^3H_6$) as a function of Tm^{3+} concentration. The peak intensity decreased with increasing Tm^{3+} molar concentration due to concentration quenching effects [26]. The highest emission was found when $x = 1$.

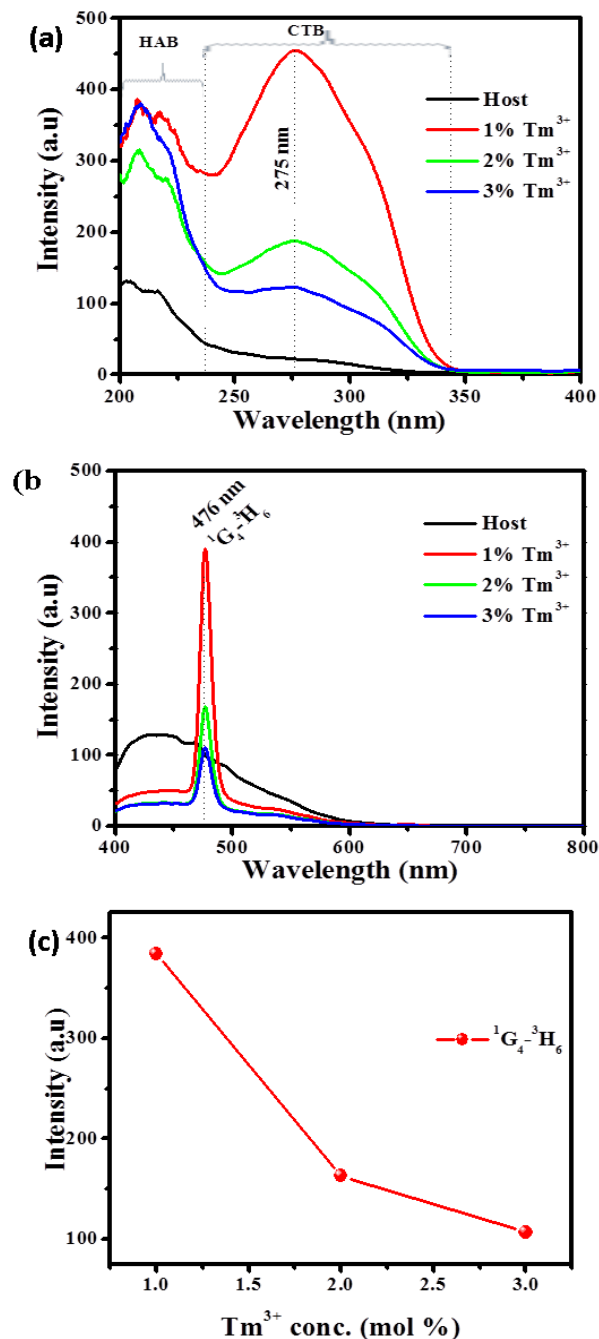


Fig. 4. (a) Excitation and (b) Emission spectra of $YV_{0.5}P_{0.5}O_4: x \text{ mol } \% Tm^{3+}$ and (c) a plot showing the intensity as a function Tm^{3+} concentration.

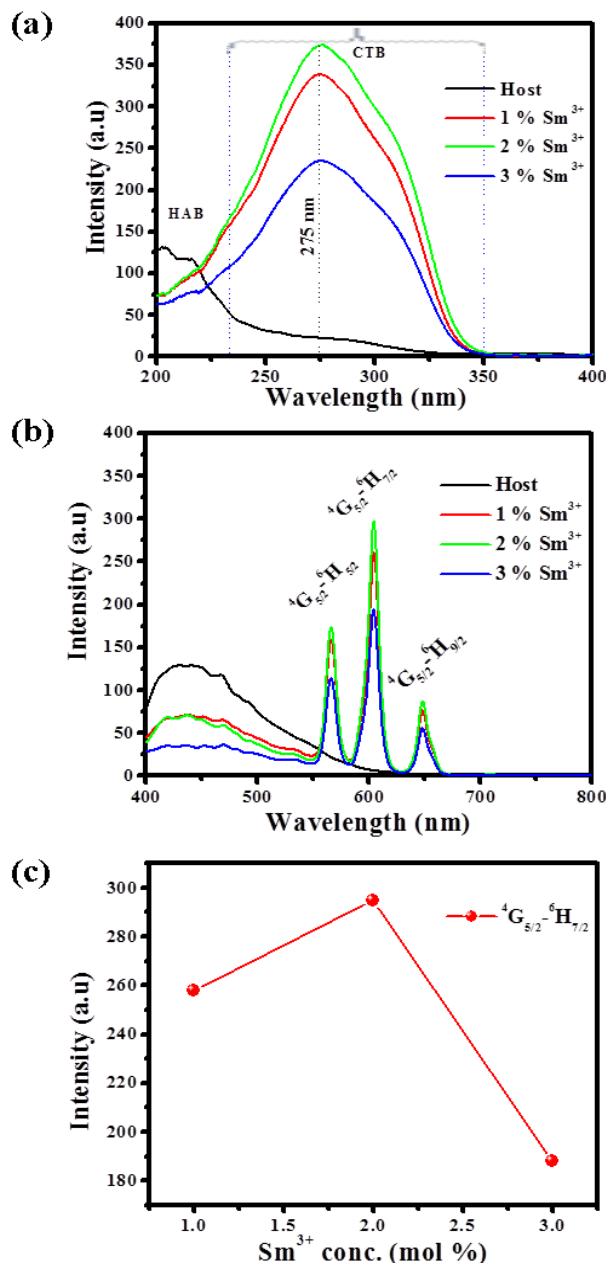


Fig. 5. (a) Excitation and (b) Emission spectra of $YV_{0.5}P_{0.5}O_4: x \text{ mol } \% Sm^{3+}$ (c) a plot showing the intensity as a function Sm^{3+} concentration.

The excitation and emission spectra of $YV_{0.5}P_{0.5}O_4: x \text{ mol } \% Sm^{3+}$ are shown in Fig. 5(a) and (b) respectively. The excitation spectra were recorded when monitoring the emission wavelength at 604 nm. The spectrum of the undoped sample shows a broad band extending from 200 to 230 nm. This band is attributed to host absorption. On the other hand, the spectra for doped samples show a strong broad band in the UV region extending from 200 to 350 nm with maximum at 275 nm. This band is due to $Sm^{3+} \rightarrow O^{2-}$ charge transfer band. The emission spectra measured under the excitation wavelength of 275 nm show four bands centered at 444, 566, 604 and 649 nm respectively. The band located at 444 nm is due to the host while other three bands are due to $(^6G_{5/2} - ^6H_{5/2})$, $(^6G_{5/2} - ^6H_{7/2})$ and $(^6G_{5/2} - ^6H_{9/2})$ transitions of Sm^{3+} respectively. The emission intensity was found to increase with an increase when concentration of Sm^{3+} was increased from 1 to

mol% and then decreased when the concentration was 3 mol% and this was probably due to concentration quenching effects. Concentration quenching is caused by an increase in the number of non-radiative transitions [27, 28].

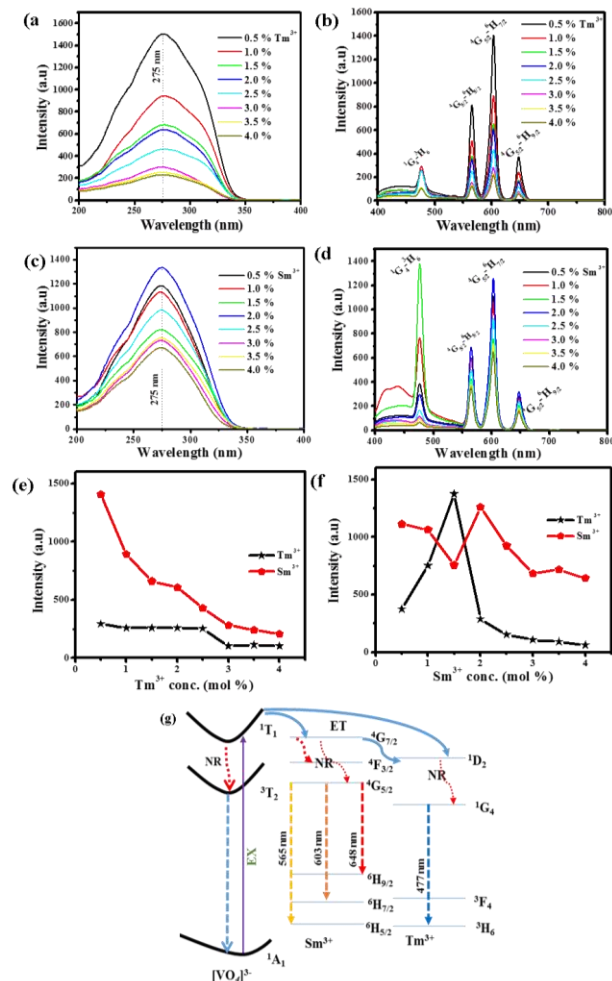


Fig. 6. (a) Excitation and (b) Emission spectra of $V_{0.5}P_{0.5}O_4$: 3 mol % Sm^{3+} , x mol % Tm^{3+} (c) Excitation and (d) Emission spectra of $YV_{0.5}P_{0.5}O_4$: 1 mol % Tm^{3+} , x mol % Sm^{3+} (e) a plot showing the intensity as a function Sm^{3+} and (f) Tm^{3+} concentration (g) Schematic representation energy level diagram and proposed mechanism.

The room temperature photoluminescence excitation spectra of $YV_{0.5}P_{0.5}O_4$: 3 mol % Sm^{3+} , x mol % Tm^{3+} and $YV_{0.5}P_{0.5}O_4$: 1 mol % Tm^{3+} , x mol % Sm^{3+} ($x = 0.5, 1.0, 1.5, 2.0$ and 2.5) phosphors are shown in **Fig. 6(a)** and **(c)**. The excitation spectra were recorded when monitoring the emission wavelength at 603 nm. A strong broad band ranging from 200 to 350 nm with the maximum at 275 nm was observed. This broad band is ascribed to charge transfer band from oxygen ligands to central vanadium in the $[VO_4]^{3-}$. The emission spectra, shown in **Fig. 6(b)** and **(d)**, comprise of five bands. The broad band extending from 400 to 650 nm originates from the host while the sharp peak at wavelength 477 nm is due to ($^1G_4 - ^3H_6$) transition of Tm^{3+} ions. The other three emission peaks observed at 566 nm ($^4G_{5/2} - ^6H_{5/2}$), 603 nm ($^4G_{5/2} - ^6H_{7/2}$) and 648 nm ($^4G_{5/2} - ^6H_{9/2}$) are due to transitions of Sm^{3+} ions. **Fig. 6 (e)** and **(f)** show the relative emission intensities of Tm^{3+} ($^1G_4 - ^3H_6$) and Sm^{3+} ($^4G_{5/2} - ^6H_{7/2}$)

as a function of molar concentration of Tm^{3+} and Sm^{3+} respectively. The increase in the molar concentration of Tm^{3+} did not make any noticeable change on the peak shape or position, but there was a significant change on the emission intensities. The emission intensity of Tm^{3+} was found to increase with an increase in the molar concentration of Tm^{3+} , while the emission intensity of Sm^{3+} was found to decrease. Similar behavior was observed with an increase in the molar concentration of Tm^{3+} or Sm^{3+} resulted in the decrease in the intensity of both Tm^{3+} and Sm^{3+} . This phenomenon suggests that there is energy transfer from Sm^{3+} to Tm^{3+} . Co-doping, in this work, played a pivotal role in the enhancement of luminescence intensity. Compared with singly doped samples, doubly doped samples have the intensity of almost three times higher. The simplified proposed mechanism is shown in **Fig. 6(g)**. The excitation ultraviolet radiation is initially absorbed by the host to promote electrons from 1A_1 , the ground to 1T_j ($j = 2, 1$), the excited state of $[VO_4]^{3-}$. Some of these excited electrons undergo a non-radiative process to 3T_j and eventually returning back to their ground state therefore emitting light, while other electrons from 3T_j transfer their energy to the $^4G_{7/2}$ levels, the excited state of Sm^{3+} , which in turn relaxed non-radiatively to $^4F_{3/2}$ and $^4G_{5/2}$ with subsequent emissions of Sm^{3+} . On the other hand, other electrons from $^4G_{7/2}$ level of Sm^{3+} transfer some of their energy to 1D_2 level, the excited state of Tm^{3+} followed by non-radiative process to 1G_4 and finally producing blue emission of Tm^{3+} .

Conclusion

In conclusion, the multicomponent structures of samarium and thulium co-activated yttrium orthovanadatephosphate were successfully synthesized by solution combustion method using urea as fuel. The XRD results indicated that the prepared nanophosphors of both singly and doubly doped $GdV_{0.5}P_{0.5}O_4$: Sm^{3+} , Tm^{3+} compounds have tetragonal structure with the peaks intermediate between that of pure YVO_4 and YPO_4 . These results further confirm that the prepared phosphor powder is a single-phase crystal. SEM and TEM images showed that the samples consisted of different sizes and shapes that include spheres, ovals and cuboids. TEM further showed well defined lattice fringes indicating that the samples are well crystalline as confirmed by XRD results. The EDS analysis showed that all the elements forming $YV_{0.5}P_{0.5}O_4$: Sm^{3+} ; Tm^{3+} were present in the compound. The UV-vis reflectance spectra had similar trend for all the samples with a broad absorption band towards ultraviolet region, except for Tm^{3+} doped samples that indicated small absorption signature at the wavelength of ~ 692 nm corresponding to $^3H_6 - ^3F_3$ transition of Tm^{3+} . The photoluminescence excitation for singly doped Tm^{3+} and Sm^{3+} and co-doped Sm^{3+} , Tm^{3+} showed a strong broad band between 200 and 350 nm peaking at $\lambda = 280, 275$ and 278 nm respectively. Tm^{3+} and Sm^{3+} singly doped samples showed one emission peak at 476 nm ($^1G_4 - ^3H_6$) and three other emission peaks at 566 ($^4G_{5/2} - ^6H_{5/2}$), 603 ($^4G_{5/2} - ^6H_{7/2}$) and 650 nm ($^4G_{5/2} - ^6H_{9/2}$)

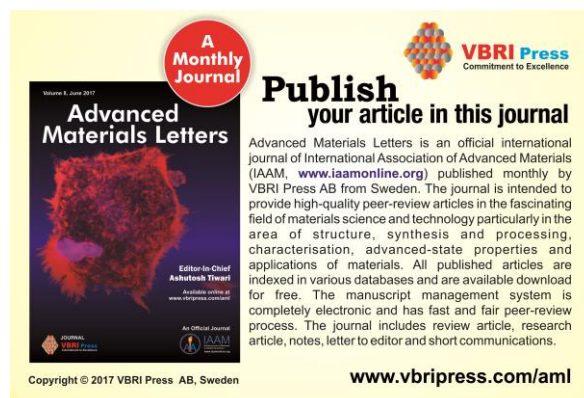
corresponding to transitions of Tm^{3+} and Sm^{3+} . Both Tm^{3+} and Sm^{3+} emission peaks were observed for co-doped samples. The PL results for co-doped phosphor indicated that an increase in Tm^{3+} molar concentration resulted in the decrease in the emission intensity of Sm^{3+} suggesting that there is energy transfer from Sm^{3+} to Tm^{3+} . The UV and photoluminescence results suggest that the prepared phosphor powder might be a suitable candidate for possible application in solar cells.

Acknowledgements

This work was by Thuthuka programme (grant No. 93936) and competitive rate research programme (grant No. CPR20110724000021870) of the National Research Foundation (NRF) of South Africa, and the rental pool programme of the National Laser Centre (NLC) of the Council for Scientific and Industrial Research (Grant No. NLC-LREGM00-CON-001).

References

- Liang, Y.; Chui, P.; Sun, X.; Zhao, Y.; Cheng, F.; Sun, K. *J. Alloys Compd.* **2013**, *552*, 289
- Cao, Y.; Liu, Y.; Feng, H.; Yang, Y. *Ceram Int.* **2014**, *40*, 15319
- Li, P.; Liu, Y.; Guo, Y.; Shi, X.; Zhu, G.; Zuo, H. *Ceram Int.* **2015**, *41*, 6620
- Li, J.; Liu, J.; Yu, X. *J. Alloys Compd.* **2011**, *509*, 9897
- He, F.; Yang, P.; Niu, N.; Wang, W.; Gai, S.; Wang, D.; Lin, J. *J. Colloid Interface Sci.* **2010**, *343*, 71
- Rivera, S.I.; Carrillo, F.J.; Garcia, A.; Oliva, J. *Mater. Lett.* **2017**, *187*, 83
- Wang, H.; Odawara, O.; Wada, H. *J. Alloys Compd.* **2016**, *683*, 1
- Zuo, Y.; Ling, W.; Wang, Y. *J. Lumin.* **2012**, *132*, 61
- Yang, Y.; Ding, M.; Song, G.; Fan, W.; Feng, H. *Chem. Phys. Lett.* **2015**, *639*, 67
- Jo, D.S.; Luo, Y.Y.; Senthil, K.; Masaki, T.; Yoon, D.H. *Opt. Mater.* **2011**, *33*, 1190
- Yu, M.; Lin, J.; Zhou, Y.H.; Pang, M.L.; Han, X.M.; Wang, S.B. *J. Thin. Sol. Film.* **2003**, *444*, 245
- Sun, J.; Xian, J.; Xia, Z.; Du, H. *J. Lumin.* **2010**, *130*, 1818
- Sue, X. Q.; Yan, B. *Mater. Chem. Phys.* **2005**, *93*, 552.
- Jin, Y.; Li, C.; Xu, Z.; Cheng, Z.; Wang, W.; Li, G.; Lin, J. *Mater. Chem. Phys.* **2011**, *129*, 418
- Na Li, N.; Sun, X.; Liu, R.; Xu, L.; Xu, K.; Song, X.M. *Sol. Energy Mat. & Sol. Cells* **2016**, *157*, 853
- Zhao, R.; Huan, L.; Gu, P.; Guo, R.; Chen, M.; Diao, G. *J. of Power Sources.* **2016**, *331*, 527
- Florencio, L.A.; Gomez-Malagon, L.A.; Lima, B.C.; Gomes, A.S.L.; Garcia, J.A.M.; Kassab L.R.P. *Sol. Energy Mat. & Sol. Cells.* **2016**, *157*, 468.
- Yao, N.; Huang, J.; Fu, K.; Deng, X.; Ding, M.; Shao, M.; Xu, X. *Electrochim. Acta.* **2015**, *154*, 273.
- Wu, J.; Wang, J.; Lin, J.; Xiao, Y.; Yue, G.; Huang, M.; Lan, Z.; Huang, Y.; Fan, L.; Yin, S.; Sato, T. *Scientific reports* **2013**, *3*: 2058.
DOI: 10.1038/srep02058
- Liu, Y.; Xiong, H.; Zhang, N.; Leng, Z.; Li, R.; Gan, S. *J. Alloys Compd.* **2015**, *653*, 126.
- Li, L.; Lui, X.G.; Noh, H.M.; Jeong, J.H. *J. Sol. State Chem.* **2015**, *221*, 95.
- Liu, X.; Li, L.; Noh, H.M.; Jeong, J.H.; Jang, K.; Shin, D.S. *J. Alloys Compd.* **2015**, *618*, 649.
- Navas, J.; Coronilla, A.S.; Aguilar, T.; De los Santos, D.M.; Hernandez, N.C.; Alcantara, R.; Lorenzo, C.F.; Calleja, J.M. *Nanoscale.* **2014**, *6*, 12740.
- Devi, C. V.; Singh, N.R. *Spectrochim. Acta Part A: Mol. Biomol. Spectrosc.* **2015**, *146*, 331.
- Barbosa, G. N.; Graeff C. F.O.; Oliveira, H. P. *Ecl. Quím., São Paulo*, **2005**, *30*, 7.
- Li, J.; Yan, H.; Yan, F. *J. Mater. Sci. Eng. B*, **2016**, *209*, 56.
- Zhao, L.; Yongfeng, W.; Jing, C.; Yuanru, J.; Xicheng, Z.; Zhixing, M. *J. Rare Earths*, **2016**, *34*, 143.
- Kuhn, S.; Herrmann, A.; Russel, C. *J. Lumin.* **2015**, *158*, 333.



A Monthly Journal

Publish your article in this journal

Advanced Materials Letters is an official international journal of International Association of Advanced Materials (IAAM, www.iaamonline.org) published monthly by VBRI Press AB from Sweden. The journal is intended to provide high-quality peer-review articles in the fascinating field of materials science and technology particularly in the area of structure, synthesis and processing, characterisation, advanced-state properties and applications of materials. All published articles are indexed in various databases and are available download for free. The manuscript management system is completely electronic and has fast and fair peer-review process. The journal includes review article, research article, notes, letter to editor and short communications.

Editor in Chief: Ashutosh Tiwari

Access online at: www.vbripress.com/aml

Copyright © 2017 VBRI Press AB, Sweden

www.vbripress.com/aml